PAPER

Check for updates

A systematic study of TMO$_n$ (TM = V, Cr, Mn, and Fe; n = 3 and 6) clusters embedded in a PtS$_2$ monolayer†

Nguyen Thanh Tien, [ID] [a] J. Guerrero-Sanchez[b] and D. M. Hoat [ID] *cd

Doping-based magnetism engineering is an effective approach to synthesize new multifunctional two-dimensional (2D) materials from their non-magnetic counterparts. In this work, doping with TMO$_n$ clusters (TM = V, Cr, Mn, and Fe; n = 3 and 6) is proposed to induce feature-rich electronic and magnetic properties in a PtS$_2$ monolayer. The pristine monolayer is a non-magnetic semiconductor with an indirect energy gap of 1.81 (2.67) eV as obtained from PBE(HSE06)-based calculations. PtS$_3$-type multivacancies magnetize significantly the monolayer, inducing the emergence of half-metallicity. In this case, a total magnetic moment of 1.90 μ_B is obtained and magnetic properties are produced mainly by atoms around the vacancy sites. Meanwhile, the PtS$_2$ monolayer is metallized by creating PtS$_6$-type multivacancies without magnetization. Depending on the type of TMO$_n$ cluster, either a feature-rich diluted magnetic semiconductor or half-metallic nature is induced, which is regulated mainly by the incorporated clusters. Except for the FeO$_6$ cluster, TM atoms and O atoms exhibit an antiparallel spin orientation, resulting in total magnetic moments between 1.00 and 4.00 μ_B. Meanwhile, the parallel spin ordering gives a large total magnetic moment of 5.99 μ_B for the FeO$_6$-doped monolayer. Furthermore, Bader charge analysis indicates that all the clusters attract charge from the host monolayer that is mainly due to the electronegative O atoms. Our results may introduce cluster doping as an efficient way to create new spintronic 2D materials from a non-magnetic PtS$_2$ monolayer.

1 Introduction

Two-dimensional (2D) magnetic materials have sparked special interest because of their importance for fundamental research as well as technological applications in the spintronic field.[1,2] In particular, intrinsic ferromagnetism has been found in CrI$_3$ (ref. 3) and Gr$_2$Ge$_2$Te$_6$ (ref. 4) nanosheets, and few-layer Fe$_3$GeTe$_2$.[5] These findings open the way for the future development of diminutive spintronic devices based on 2D materials. Note that the mentioned materials contain transition metals as constituent atoms, which produce mainly their intrinsic magnetism. Meanwhile, most of the 2D materials discovered until now lack inherent magnetism. Therefore, researchers have made extensive efforts to introduce magnetism into these non-magnetic counterparts. In this regard, various strategies have been

proposed encompassing defect engineering,[6–8] doping,[9–11] surface modification,[12–14] and edge cutting to form nanoribbons.[15–17] Among them, substitutional doping has been widely employed as a simple and effective technique for inducing magnetization in 2D materials, validated by both theoretical and experimental investigations. Experimentally, doping processes have been successfully realized by either ion implantation[18,19] or chemical vapor deposition.[20,21] Theoretically, first-principles calculations have demonstrated that not only transition metals[22,23] but also non-transition metals or even non-metals impurities can induce significant magnetism in non-magnetic 2D materials.[24–27]

On the other hand, 2D layered transition metal dichalcogenides (TMDs) have been widely explored due to their potential for electronic and optoelectronic applications.[28,29] Unlike the semimetal behavior of graphene, TMD monolayers are semiconductors with sizable electronic band gaps between 1 and 3 eV. Initially, research was focused on those TMDs based on the VIB group (Mo and W atoms), which have been synthesized by both top-down (exfoliation from their bulk counterparts) and bottom-up (Chemical Vapor Deposition – CVD) methods.[30–33] Recently, as new members of the 2D TMD family, noble metal dichalcogenides have drawn great research attention as promising candidates for different applications including optoelectronics,[34] mid-infrared photonics,[35] and photocatalysis,[36]

a College of Natural Sciences, Can Tho University, 3-2 Road, Can Tho City 900000, Vietnam

b Universidad Nacional Autónoma de México, Centro de Nanociencias y Nanotecnología, Apartado Postal 14, Código Postal 22800, Ensenada, Baja California, Mexico

c Institute of Theoretical and Applied Research, Duy Tan University, Ha Noi 100000, Vietnam. E-mail: dominhhoat@duytan.edu.vn

d Faculty of Natural Sciences, Duy Tan University, Da Nang 550000, Vietnam

† Electronic supplementary information (ESI) available. See DOI: https://doi.org/10.1039/d4na00465e

among others. Among them, platinum sulfide (PtS_2) has been investigated both experimentally and theoretically. Large-scale few-layer PtS_2 films have been synthesized by Zhao et al.[37] by means of the direct sulfurization of pre-deposited Pt. The synthesized materials exhibit p-type transport behavior with uniform electrical performance. Similarly, Lu et al.[38] have also realized the synthesis of large-scale uniform few-layer PtS_2 in a plasma enhanced CVD furnace, where a field-effect transistor (FET) fabricated on few-layer PtS_2 shows a p-type semiconductor behavior. Using first-principles calculations, Villaos et al.[39] have demonstrated that the PtS_2 band gap increases according to reduce its thickness, from 0.25 eV of bulk counterpart to 1.68 eV of monolayer counterpart. Moreover, several research groups have studied the modification of PtS_2 monolayer electronic and magnetic properties using external strain[40] and vacancies.[41]

It is well known that doping is an efficient way to change the physical properties of 2D materials.[42] Beyond monoelement substitution, doping with multielement impurities has also been proposed to tailor charge and magnetic states. For example, feature-rich electronic and magnetic properties can be induced in a MoS_2 monolayer by doping with transition metal trioxides – TMO_3 (TM = 3d transition metals)[43] or FeX_6 clusters (X = S, C, N, O, F).[44] Similarly, magnetic functionalization of graphene is also achieved by doping with TMO_3 clusters to form new promising spintronic 2D materials.[45] Motivated by these findings, we investigate the effects of transition metal oxide TMO_n (TM = V, Cr, Mn, and Fe; n = 3 and 6) clusters on the PtS_2 monolayer electronic and magnetic properties. The modified electronic properties are studied using the spin-polarized band structure and density of states, while the difference in spin-dependent charge distributions confirms the induced magnetism. It is anticipated that our results indicate the emergence of novel feature-rich electronic and magnetic properties in the PtS_2 monolayer by doping with TMO_n clusters towards creating potential spintronic 2D materials.

2 Computational details

Density Functional Theory (DFT)-based calculations[46] are performed using the Vienna ab initio Simulation Package (VASP),[47,48] which makes use of the Projector Augmented Wave (PAW) method. Electron exchange-correlation potential is treated using the Perdew–Burke–Ernzerhof scheme of the Generalized Gradient Approximation (GGA-PBE).[49] In combination with the DFT + U method reported by Dudarev et al.,[50] the finite on-site Coulomb interactions of highly correlated 3d electrons of transition metals are considered using effective Hubbard parameters U_{eff} of 3.25, 3.70, 3.90, and 5.40 eV for V, Cr, Mn, and Fe atoms,[51,52] respectively. For the expansion of the basis set, the cutoff energy is chosen as 500 eV. For self-consistent iterations, the total energy is set to converge to 1×10^{-6} eV. The structures are relaxed until the forces on each atom have converged to 1×10^{-2} eV $Å^{-1}$. A vacuum layer wider than 14 Å – perpendicular to the monolayer plane – is inserted (along the z-axis) to ensure the negligible interactions between periodic images.

In order to investigate the effects of vacancies and doping with clusters in the PtS_2 monolayer, a $4 \times 4 \times 1$ supercell with 48 atoms is constructed. Herein, the Brillouin zone is sampled with a $4 \times 4 \times 1$ Γ-centered Monkhorst–Pack k-mesh.[53] Meanwhile, a denser k-mesh of $20 \times 20 \times 1$ is utilized for the pristine monolayer with 3 atoms in the unit cell. Then, the formation energy E_f is calculated as follows:

$$E_f = E_t - E_m + \sum_i n_i \mu_i - \sum_j n_j \mu_j \qquad (1)$$

where E_t and E_m are the total energy of the defected/doped and pristine PtS_2 monolayers, respectively; n and μ denote the number of replaced host atoms (i)/incorporated atoms (j) and their chemical potential, respectively. In addition, the cohesive energy E_c of each system is also computed using the following expression:

$$E_c = \frac{E_t - [m_{Pt}E(Pt) + m_S E(S) + m_{TM}E(TM) + m_O E(O)]}{m_{Pt} + m_S + m_{TM} + m_O} \qquad (2)$$

Herein, m_X is the number of atoms X in the system; $E(X)$ refers to the energy of an isolated X atom.

The electronic interactions between the host monolayer and clusters are investigated by means of Bader charge analysis,[54,55] which provides information about the charge transfer. In addition, the charge density difference $\Delta\rho$ is obtained from cleaving separately the host monolayer and cluster from the doped systems as follows:

$$\Delta\rho = \rho(TMO_x + PtS_2) - \rho(PtS_2) - \rho(TMO_x) \qquad (3)$$

In this equation, the terms on the right hand side denote the charge density of the doped system, the charge density of the host monolayer, and the charge density of the cluster, respectively.

3 Results and discussion

3.1 Pristine PtS_2 monolayer

As a first step, the PtS_2 monolayer geometry is optimized. Fig. 1 shows the optimized unit cell, which is fully described by the following structural parameters: (1) lattice constant $a = 3.57$ Å, which is in good agreement with previous calculations;[56] (2) chemical bond length $d_{Pt-S} = 2.40$ Å; (3) total buckling height $\Delta_{total} = 2 \times \Delta_{Pt-S} = 2 \times 1.23 = 2.46$ Å; (4) interatomic angles $\angle PtSPt = 96.20°$ and $\angle SPtS = 83.80°$. Then, the stability of the PtS_2 monolayer is examined using the following criteria:

• The phonon dispersion curves are calculated using the PHONOPY code.[57] The results plotted in Fig. 2a show no obvious nonphysical imaginary frequency in the entire Brillouin zone, indicating that the PtS_2 monolayer is dynamically stable.

• Ab initio Molecular Dynamics (AIMD) simulations are performed at 300 K for 5 ps, using a $4 \times 4 \times 1$ supercell. Herein, the NVT ensemble and Nose–Hoover thermostat are utilized.[58,59] Fig. 2b shows the variation of temperature and the final atomic structure. The stable fluctuation of temperature around 300 K can be noted. Moreover, no geometry reconstruction or broken
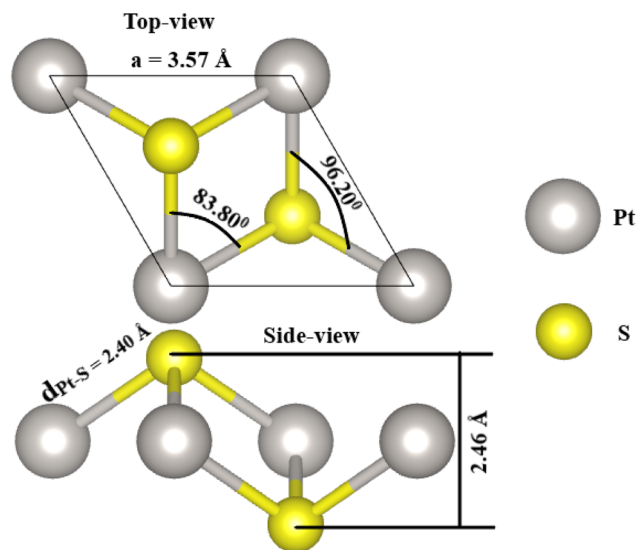
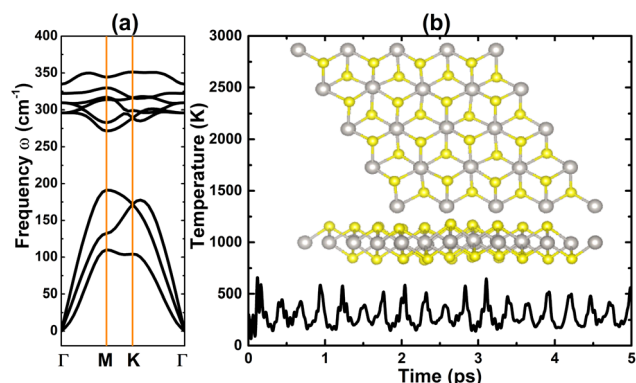Fig. 1 Optimized unit cell of the PtS_2 monolayer.

Fig. 2 (a) Phonon dispersion curves and (b) AIMD simulations (variation of temperature + final atomic structure) at 300 K of the PtS_2 monolayer.

Pt–S chemical bonds are noted, indicating that the structure is well preserved. These results indicate that the PtS_2 monolayer is thermally stable.

● Using the energy-strain method, the elastic constants of the PtS_2 monolayer are calculated. According to our calculations, its C_{11} and C_{12} constants have values of 88.57 and 23.26 N m^{-1}, respectively, which can describe well the elasticity of 2D hexagonal symmetry. Importantly, the obtained elastic constants satisfy Born's criteria:[60] $C_{11} > 0$ and $C_{11} > |C_{12}|$, indicating that the PtS_2 monolayer is mechanically stable.

The electronic properties as well as interactions between the Pt and S atoms of the PtS_2 monolayer are investigated using the optimized atomic structure. Fig. 3a shows the band structures obtained from PBE- and HSE06-based calculations. The HSE06 functional with a 25% fraction of the exact Hartree exchange potential is also utilized to calculate more accurately the monolayer band gap.[61] Since the valence band maximum and conduction band minimum are located at different points as determined by both functionals, the PtS_2 monolayer can be
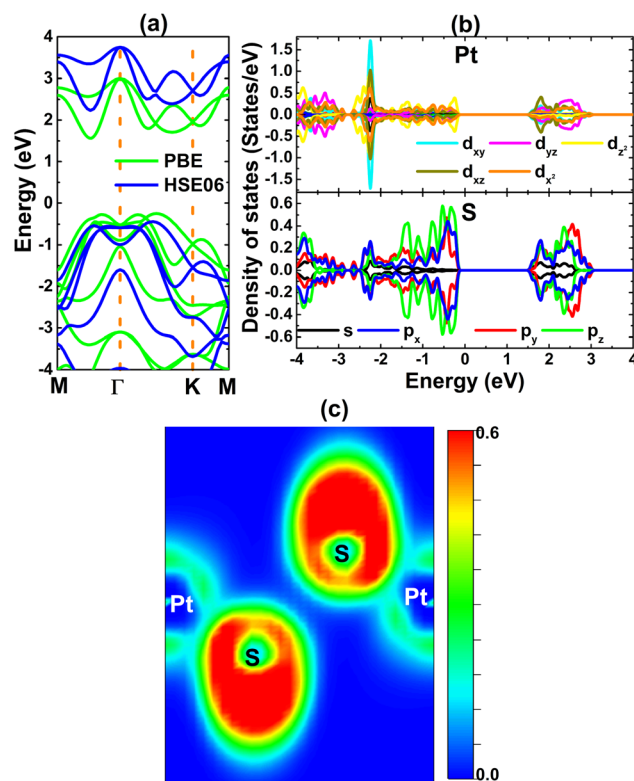

Fig. 3 (a) Electronic band structure (the Fermi level is set to 0 eV), (b) projected density of states, and (c) electron localization function of the PtS_2 monolayer.

classified as a 2D indirect-gap semiconductor. The standard PBE functional provides an energy gap of 1.81 eV, while a larger (expected to be more accurate) value of 2.67 eV is obtained from HSE06-based computation. Note that these energy gaps are in line with results reported previously by several research groups,[39,62] suggesting the reliability of our calculations. The projected density of states (PDOS) of both Pt and S atoms is given in Fig. 3b to analyze their contribution. Significant contributions of Pt-5d and S-3p orbitals in the considered energy range around the Fermi level can be noted. Moreover, their electronic states exhibit significant hybridization in both the valence band and the conduction band, giving evidence of the covalent Pt–S chemical bond. However, the difference in electronegativity between Pt and S atoms may cause charge transfer, forming ionic bonds. Specifically, Bader charge analysis implies that each S atom attracts a charge of 0.21 e from the Pt atom. Therefore, it can be concluded that the Pt–S chemical bonds in the PtS_2 monolayer exhibit a mix of ionic and covalent characteristics.

3.2 Effects of PtS_3- and PtS_6-type multivacancies

In this part, the effects of PtS_3- and PtS_6-type multivacancies (Va_{PtS_3} and Va_{PtS_6} systems) on the PtS_2 monolayer electronic and magnetic properties are investigated. The atomic structures of these defected systems are visualized in Fig. S1 of the ESI.† Table 1 shows E_f values of 7.38 and 12.64 eV for Va_{PtS_3} and Va_{PtS_6} systems, respectively. These values correspond to 1.85 and 1.81 eV per atom for each single vacancy, respectively. The PtS_2

Table 1 Formation energy E_f (eV), cohesive energy E_c (eV per atom), electronic band gap E_g (eV; spin-up/spin-down; M: metallic), charge transferred from the host monolayer to the cluster ΔQ (e), total magnetic moment M_t (μ_B), and local magnetic moment M_l of the cluster (μ_B, TM/O) of the defected/doped PtS_2 monolayer

	E_f	E_c	E_g	ΔQ	M_t	M_l
Va_{PtS_3}	7.38	−4.41	M/0.42	—	1.90	—
Va_{PtS_6}	12.64	−4.37	M/M	—	0.00	—
D_{VO_3}	−2.06	−4.53	M/1.27	0.76	1.00	0.83/−0.08
D_{CrO_3}	−1.52	−4.45	0.83/1.25	0.85	2.00	2.37/−0.13
D_{MnO_3}	−1.36	−4.47	0.80/1.17	1.07	3.00	3.80/−0.08
D_{FeO_3}	−0.36	−4.49	M/1.16	1.07	4.00	3.92/0.02
D_{VO_6}	−3.41	−4.57	1.23/1.49	2.99	1.00	1.12/−0.03
D_{CrO_6}	−2.81	−4.49	M/1.51	3.17	2.00	2.79/−0.11
D_{MnO_6}	−1.81	−4.49	1.52/0.82	3.03	3.00	3.76/−0.14
D_{FeO_6}	−1.05	−4.52	1.52/0.09	3.06	5.99	4.27/0.20

monolayer exhibits good structural and chemical stability under the effects of multivacancies, which is confirmed by negative E_c values of −4.41 and −4.37 eV per atom, respectively. However, these values are less negative than that of the perfect PtS_2 monolayer (−4.53 eV per atom), suggesting a slight reduction in the stability.

Significant magnetization of the PtS_2 monolayer induced by creating PtS_3-type multivacancies is found. The emergence of magnetism is confirmed by the difference in charge distribution between spin channels. Specifically, this difference leads to a total magnetic moment of 1.90 μ_B. The spin density illustrated in Fig. 4 indicates that the magnetic properties of the Va_{PtS_3} system are produced mainly by first S atoms from vacancy sites, where a small contribution from second Pt atoms and third S atoms is also observed. In contrast, no magnetism is obtained for the Va_{PtS_6} system, indicating the preservation of the non-magnetic nature of the PtS_2 monolayer when creating PtS_6-type nanoholes.

Fig. 5 shows the spin-polarized band structures of Va_{PtS_3} and Va_{PtS_6} systems. From the figure, one can see new middle-gap
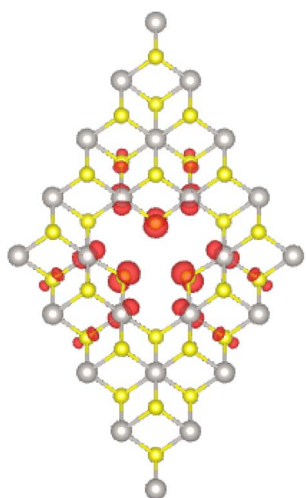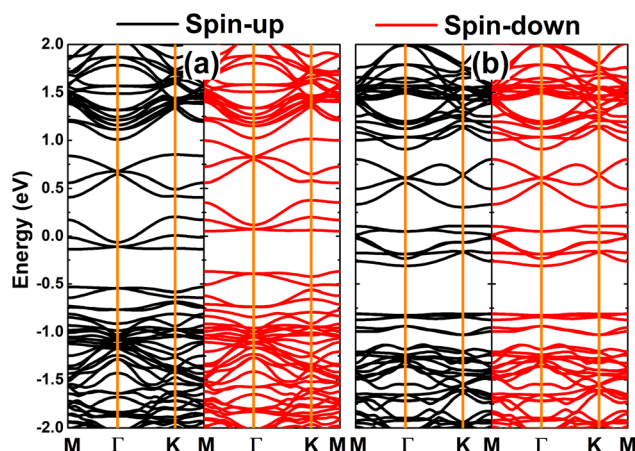

Fig. 5 Spin-polarized band structure (the Fermi level is set to 0 eV) of the PtS_2 monolayer with (a) PtS_3- and (b) PtS_6-type vacancies.

energy states created by vacancy defects that determine the system electronic behavior. It is important to mention that the unbalanced charge distribution is also reflected in the spin polarization of the Va_{PtS_3} system band structure, while that of the Va_{PtS_6} system is totally symmetric. These profiles are in agreement with the above analysis of magnetism. One of the PtS_2 monolayer spin states is metallized under the effects of PtS_3-type multivacancies, while the semiconductor character is preserved in the other one. Therefore, the Va_{PtS_3} system can be classified as a 2D half-metallic material. Thus, creating PtS_3-type multivacancies is an effective method to functionalize PtS_2 monolayers for spintronic applications.[63] In contrast, the Va_{PtS_6} system exhibits a non-magnetic metallic nature considering the metallization of both spin states.

The origin of middle-gap states is studied through the PDOS spectra of Pt and S atoms closest to vacancy sites. From Fig. 6a, one can see that the spin-up metallic character of the Va_{PtS_3} system is generated mainly by Pt-d_{xy}, Pt-d_{yz}, and S-p_z states. The spin-down band gap is regulated by the hybridization between Pt-d_{xz} and S-p_z states, which also produces the system magnetism as suggested by their strong spin polarization in the vicinity of the Fermi level. In the case of the Va_{PtS_6} system, Pt-d_{yz} and S-p_z states cause mainly monolayer metallization (see Fig. 6b).
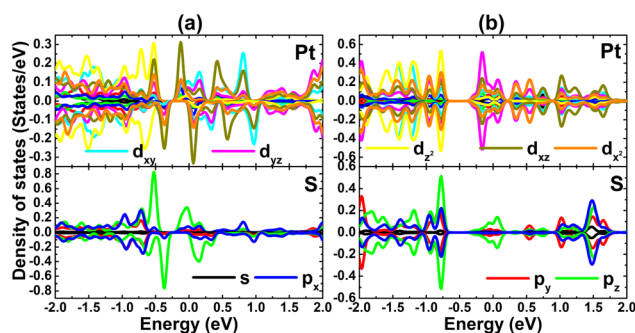

Fig. 4 Spin density (iso-surface value: 0.005 e Å^{-3}) in the PtS_2 monolayer with PtS_3-type vacancies.

Fig. 6 Projected density of states of atomic species around the defect sites of the PtS_2 monolayer with (a) PtS_3- and (b) PtS_6-type vacancies.

3.3 Effects of doping with TMO₃ clusters

Herein, the effects of doping with TMO_3 (D_{TMO_3} system) clusters on the PtS_2 monolayer electronic and magnetic properties are investigated. The calculated formation energy and cohesive energy are given in Table 1. Our calculations provide negative E_f values of −2.06, −1.52, −1.36, and −0.36 eV for D_{VO_3}, D_{CrO_3}, D_{MnO_3}, and D_{FeO_3} systems, respectively. These results indicate the exothermic character of the doping process. The doping process is less favorable according to the increase of the atomic number of transition metals since the formation energy becomes less negative in this direction. Moreover, negative E_c values between −4.53 and −4.45 eV per atom imply that all four D_{TMO_3} systems are structurally and chemically stable, where the incorporation of clusters reduces only slightly the monolayer stability.

Our calculations confirm the significant magnetization of the PtS_2 monolayer upon doping with TMO_3 clusters. Total magnetic moments of 1.00, 2.00, 3.00, and 4.00 μ_B are obtained for D_{VO_3}, D_{CrO_3}, D_{MnO_3}, and D_{FeO_3} systems, respectively. As expected, the system magnetism is produced mainly by TM atoms as suggested by the illustration of spin density in Fig. 7. From the figure, one can see large spin surfaces centered at TM sites. Moreover, small iso-surfaces are also observed near O and S atoms, indicating their small contribution to the system magnetism. It is important to note the antiparallel spin orientation between TM atoms and their neighboring O and S atoms.

The magnetism of D_{TMO_3} systems is also reflected in the spin polarization as observed in their band structures displayed in Fig. 8. The electronic nature of the doped systems is determined by doping-induced middle-gap energy states. Specifically, D_{VO_3} and D_{FeO_3} are half-metallic 2D systems considering their metallic spin-up state and semiconductor spin-down state. Herein, the spin-down energy gaps of 1.27 and 1.16 eV are obtained, respectively. Additionally, a diluted magnetic semiconductor nature emerges in the PtS_2 monolayer when doping with CrO_3 and MnO_3 clusters. In these cases, the spin-up/spin-down band gaps of 0.83/1.25 and 0.80/1.17 eV are obtained for D_{CrO_3} and D_{MnO_3} systems, respectively. These results suggest that feature-rich electronic and magnetic properties desired for spintronic applications can be induced in the PtS_2 monolayer by doping with TMO_3 clusters.[64]

The calculated charge density difference confirms the charge depletion at TM atoms and charge accumulation at their neighboring O and S atoms (see Fig. S2 of the ESI†). The Bader charge is analyzed focusing on the constituent atoms of clusters. It is found that V, Cr, Mn, and Fe atoms lose charge amounts of 1.76, 1.61, 1.45, and 1.42 e, respectively. Meanwhile, each O atom of VO_3, CrO_3, MnO_3, and FeO_3 clusters gains a charge of 0.84, 0.82, 0.84, and 0.83 e, respectively. Therefore, it can be concluded that the host monolayer loses charge, transferring 0.76, 0.85, 1.07, and 1.07 e to VO_3, CrO_3, MnO_3, and FeO_3 clusters, respectively.

Fig. 9 shows the PDOS spectra of TM and O atoms of the clusters to study their contribution in the vicinity of the Fermi level, where TM-3d and O-2p orbitals are most prominent. Note that TM-$d_{xy} - d_{yz} - d_{z^2}$ and P-p_z states primarily contribute to
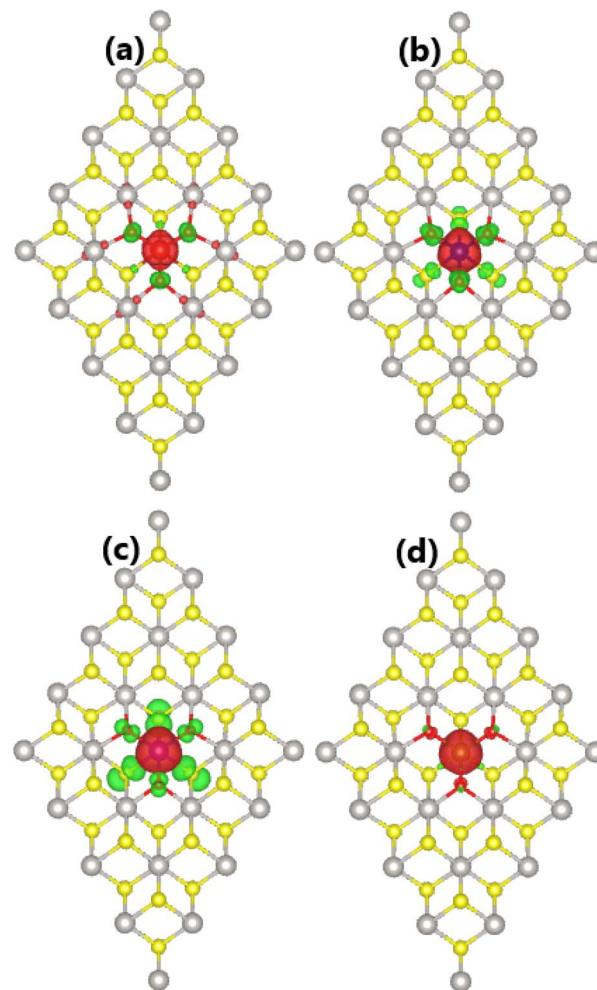

Fig. 7 Spin density (iso-surface value: 0.005 e Å⁻³; red surface: positive spin value; green surface: negative spin value) in the PtS_2 monolayer doped with (a) VO_3, (b) CrO_3, (c) MnO_3, and (d) FeO_3 clusters.

the metallic character of the spin-up state in the D_{VO_3} and D_{FeO_3} systems. As expected, the 3d orbital of transition metals exhibits strong spin polarization around the Fermi level to confirm their key role in producing the system magnetism.

3.4 Effects of doping with TMO₆ clusters

Now, the effects of doping with TMO_6 (D_{TMO_6} system) clusters on the PtS_2 monolayer electronic and magnetic properties are investigated. Similar to previous cases of doping with TMO_3 clusters, negative E_f values suggest an exothermic doping process. Specifically, E_f values of −3.41, −2.81, −1.81, and −1.05 eV are obtained for D_{VO_6}, D_{CrO_6}, D_{MnO_6}, and D_{FeO_6} systems, respectively. Note that the formation energy becomes less negative when switching the transition metal from V to Fe, indicating the reduction of energetic favorability in this direction. Once formed, all the doped systems may have good structural and chemical stability as suggested by negative E_c values between −4.57 and −4.49 eV per atom, which are quite similar to that of the bare PtS_2 monolayer.
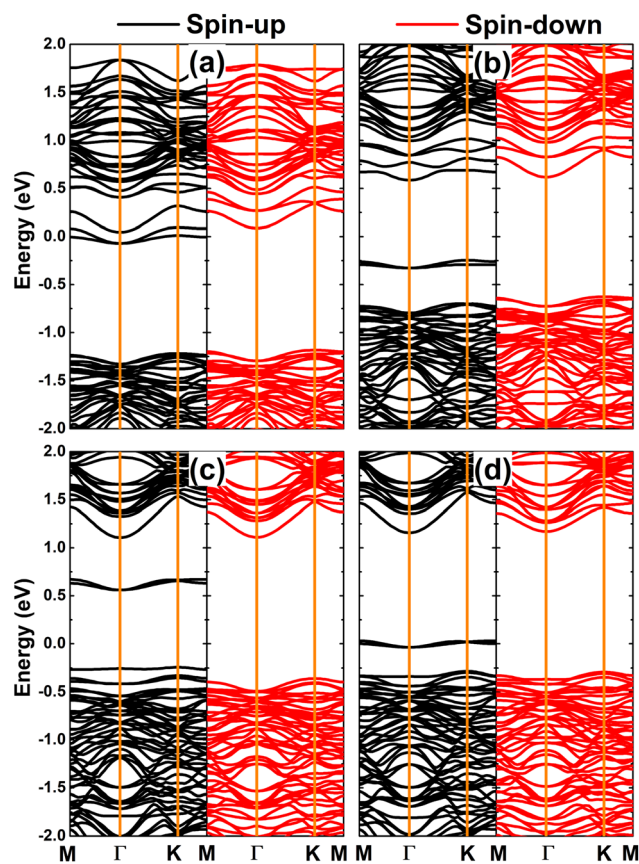
Fig. 8 Spin-polarized band structure (the Fermi level is set to 0 eV) of the PtS_2 monolayer doped with (a) VO_3, (b) CrO_3, (c) MnO_3, and (d) FeO_3 clusters.
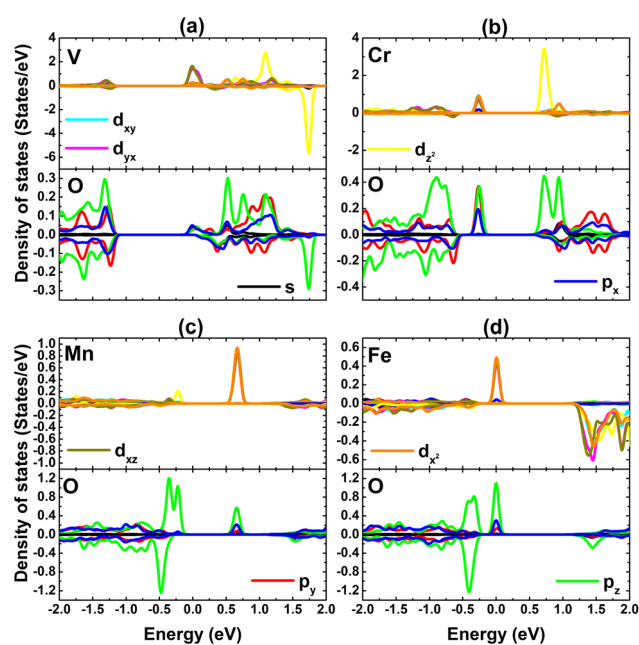

Fig. 9 Projected density of states of cluster atomic species of the PtS_2 monolayer doped with (a) VO_3, (b) CrO_3, (c) MnO_3, and (d) FeO_3 clusters.

By calculating the difference in charge distribution between spin configurations, total magnetic moments of 1.00, 2.00, 3.00, and 5.99 μ_B are obtained for D_{VO_6}, D_{CrO_6}, D_{MnO_6}, and D_{FeO_6} systems, respectively. Fig. 10 illustrates the spin density in these cluster-doped systems, which confirms that magnetic properties are produced mainly by the incorporated clusters. The iso-surface size indicates the key role of transition metals, where a smaller contribution from O atoms is also noted. Note that TM atoms and O atoms in D_{VO_6}, D_{CrO_6} and D_{MnO_6} systems exhibit an antiparallel spin orientation. In contrast, parallel spin ordering is observed for Fe atoms and O atoms in the D_{FeO_6} system, resulting in a total magnetic moment that is much larger than that of the remaining three systems.

According to the emergence of the magnetism in the PtS_2 monolayer, doping with TMO_6 clusters leads to strong spin polarization in the electronic band structures as displayed in Fig. 11. Note that the spin symmetry breaking takes place mainly in the vicinity of the Fermi level of D_{TMO_6} systems, where new middle-gap energy branches regulate their system
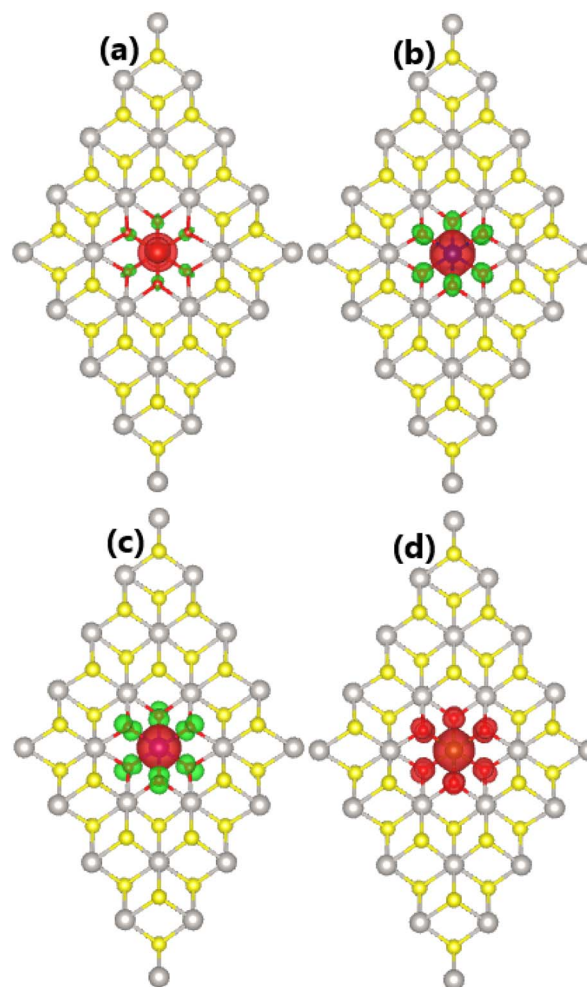

Fig. 10 Spin density (iso-surface value: 0.005 e Å^{-3}; red surface: positive spin value; green surface: negative spin value) in the PtS_2 monolayer doped with (a) VO_6, (b) CrO_6, (c) MnO_6, and (d) FeO_6 clusters.

electronic nature. The band structure profiles imply the diluted magnetic semiconductor nature of D_{VO_6}, D_{MnO_6} and D_{FeO_6} systems. In these cases, spin-up/spin-down energy gaps of 1.23/1.49, 1.52/0.82, and 1.52/0.09 eV are obtained, respectively. Moreover, the feature-rich half-metallicity is achieved by doping with CrO_6 clusters, where the D_{CrO_6} system has a metallic spin-up state and a semiconductor spin-down state with an energy gap of 1.51 eV. Such diluted magnetic semiconductor and half-metallic characteristics make D_{TMO_6} systems prospective 2D candidates for spintronic applications.[64]

To investigate the interactions between clusters and their environment, the charge density difference is calculated. Charge depletion at TM sites and those Pt atoms around clusters is found, while charge enrichment is noted at O sites (see Fig. S3 of the ESI†). This feature indicates the charge gaining of O atoms, which is because of their more electronegative nature as compared to TM and Pt atoms. Focusing on the clusters, our Bader charge analysis indicates that the TM/O atoms of VO_6, CrO_6, MnO_6, and FeO_6 cluster have an effective ionic charge of +1.93/−0.82, +1.63/−0.80, +1.71/−0.79, and +1.74/−0.80 e ("+": charge losing; "−": charge gaining), respectively. The results indicate that these clusters gain a charge of −2.99, −3.17, −3.03, and −3.06 e from the host PtS_2 monolayer, respectively.
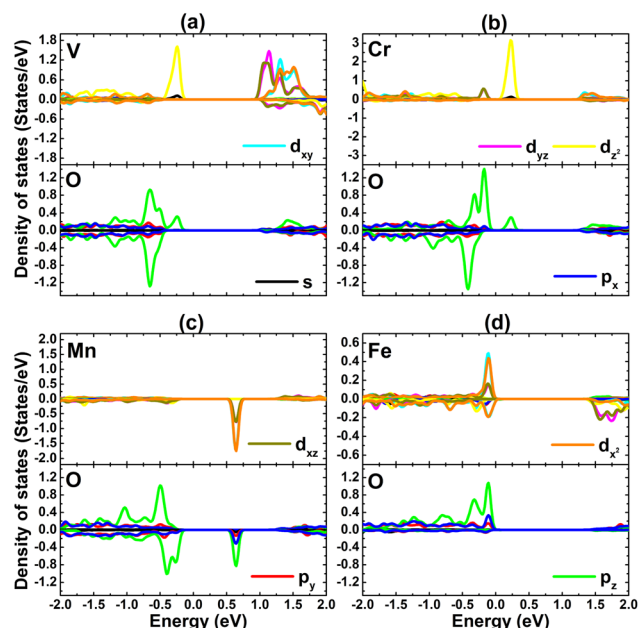

Fig. 12 Projected density of states of cluster atomic species of the PtS_2 monolayer doped with (a) VO_6, (b) CrO_6, (c) MnO_6, and (d) FeO_6 clusters.

The PDOS spectra of TM and O atoms are given in Fig. 12. In the considered energy range, TM-3d and O-2p orbitals make the main contributions. The metallic character of the D_{CrO_3} system spin-up state is derived mainly from the O-p_z state. The degree of spin polarization also indicates the key role of TM atoms in producing magnetic properties, with additional contributions coming from the p_z state of their neighboring O atoms.

4 Conclusions

In summary, the effects of doping with TMO_n clusters on the electronic and magnetic properties of PtS_2 monolayers have been systematically investigated using first-principles calculations. The dynamical, thermal, and mechanical stability of the PtS_2 monolayer is confirmed. It is a 2D indirect-gap semiconductor material, whose Pt–S chemical bonds exhibit a mix of covalent and ionic characteristics. The non-magnetic nature is preserved by creating PtS_6-type multivacancies, where the monolayer becomes a metallic 2D material. In contrast, significant magnetism is achieved under the effects of PtS_3-type multivacancies, where the p_z state of S atoms around the vacancy sites is primarily responsible for magnetic properties. Interestingly, feature-rich half-metallicity is obtained for the Va_{PtS_3} system. Similarly, the monolayer is significantly magnetized by doping with TMO_n clusters. Feature-rich diluted magnetic semiconductor or half-metallic behaviors are obtained, depending on the nature of TMO_n clusters. In these cases, electronic and magnetic properties are regulated mainly by TM-3d and O-2p orbitals. An antiparallel spin orientation in VO_3, CrO_3, MnO_3, FeO_3, VO_6, CrO_6, and MnO_6 clusters has also been found, resulting in total magnetic moments between 1.00 and 4.00 μ_B. Meanwhile, the FeO_6 cluster exhibits parallel spin
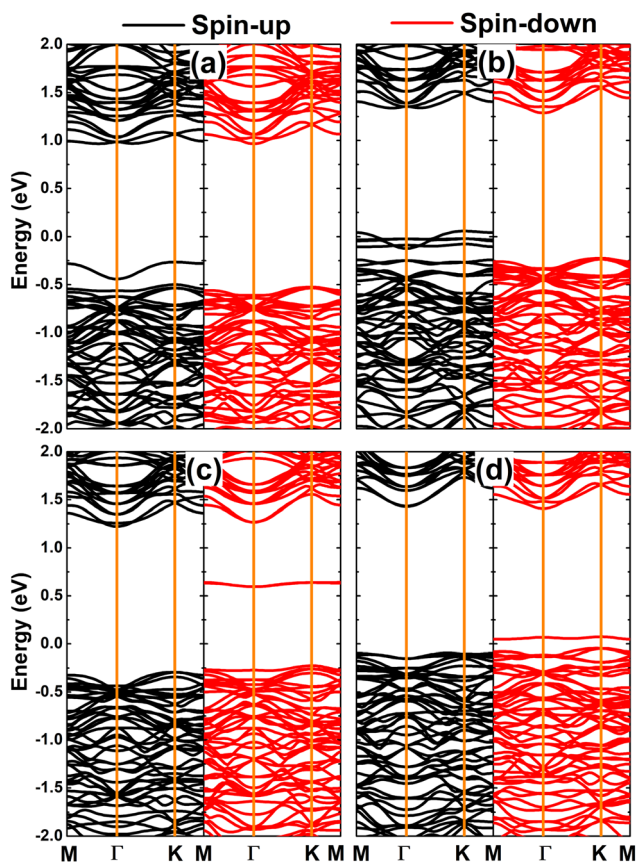

Fig. 11 Spin–polarized band structure (the Fermi level is set to 0 eV) of the PtS_2 monolayer doped with (a) VO_6, (b) CrO_6, (c) MnO_6, and (d) FeO_6 clusters.

ordering, resulting in a large total magnetic moment of 5.99 μ_B. Once incorporated substitutionally into the PtS_2 monolayer, TMO_n clusters act as charge gainers, attracting significant charge from the host monolayer. Our study suggests that new potential spintronic 2D materials can be made from PtS_2 monolayers through doping with TMO_n clusters.

Data availability

Data related to this study are available upon reasonable request.

Conflicts of interest

The authors declare that they have no known competing financial interests or personal relationships that could have appeared to influence the work reported in this paper.

Acknowledgements

References

1 E. C. Ahn, 2D materials for spintronic devices, *npj 2D Mater. Appl.*, 2020, **4**(1), 17.

2 Y. P. Feng, L. Shen, M. Yang, A. Wang, M. Zeng, Q. Wu, S. Chintalapati and C.-R. Chang, Prospects of spintronics based on 2D materials, *Wiley Interdiscip. Rev.: Comput. Mol. Sci.*, 2017, **7**(5), e1313.

3 B. Huang, G. Clark, E. Navarro-Moratalla, D. R. Klein, R. Cheng, K. L. Seyler, D. Zhong, E. Schmidgall, M. A. McGuire, D. H. Cobden, *et al.*, Layer-dependent ferromagnetism in a van der Waals crystal down to the monolayer limit, *Nature*, 2017, **546**(7657), 270–273.

4 C. Gong, L. Li, Z. Li, H. Ji, A. Stern, Y. Xia, T. Cao, W. Bao, C. Wang, Y. Wang, *et al.*, Discovery of intrinsic ferromagnetism in two-dimensional van der Waals crystals, *Nature*, 2017, **546**(7657), 265–269.

5 Y. Deng, Y. Yu, Y. Song, J. Zhang, N. Z. Wang, Z. Sun, Y. Yi, Y. Z. Wu, S. Wu, J. Zhu, *et al.*, Gate-tunable room-temperature ferromagnetism in two-dimensional Fe_3GeTe_2, *Nature*, 2018, **563**(7729), 94–99.

6 Z. Lin, B. R. Carvalho, E. Kahn, R. Lv, R. Rao, H. Terrones, M. A. Pimenta and M. Terrones, Defect engineering of two-dimensional transition metal dichalcogenides, *2D Materials*, 2016, **3**(2), 022002.

7 A. Avsar, A. Ciarrocchi, M. Pizzochero, D. Unuchek, O. V. Yazyev and A. Kis, Defect induced, layer-modulated magnetism in ultrathin metallic $PtSe_2$, *Nat. Nanotechnol.*, 2019, **14**(7), 674–678.

8 O. V. Yazyev and L. Helm, Defect-induced magnetism in graphene, *Phys. Rev. B*, 2007, **75**(12), 125408.

9 D. Shen, B. Zhao, Z. Zhang, H. Zhang, X. Yang, Z. Huang, B. Li, R. Song, Y. Jin, R. Wu, *et al.*, Synthesis of group VIII magnetic transition-metal-doped monolayer $MoSe_2$, *ACS Nano*, 2022, **16**(7), 10623–10631.

10 M. Fan, J. Wu, J. Yuan, L. Deng, N. Zhong, L. He, J. Cui, Z. Wang, S. K. Behera, C. Zhang, *et al.*, Doping nanoscale graphene domains improves magnetism in hexagonal boron nitride, *Adv. Mater.*, 2019, **31**(12), 1805778.

11 K. Kang, S. Fu, K. Shayan, Y. Anthony, S. Dadras, X. Yuzan, F. Kazunori, M. Terrones, W. Zhang, S. Strauf, *et al.*, The effects of substitutional Fe-doping on magnetism in MoS_2 and WS_2 monolayers, *Nanotechnology*, 2020, **32**(9), 095708.

12 V. V. Kulish, O. I. Malyi, C. Persson and P. Wu, Adsorption of metal adatoms on single-layer phosphorene, *Phys. Chem. Chem. Phys.*, 2015, **17**(2), 992–1000.

13 O. Üzengi Aktürk, E. Aktürk and S. Ciraci, Effects of adatoms and physisorbed molecules on the physical properties of antimonene, *Phys. Rev. B*, 2016, **93**(3), 035450.

14 W. Li, M. Zhao, Y. Xia, R. Zhang and Y. Mu, Covalent-adsorption induced magnetism in graphene, *J. Mater. Chem.*, 2009, **19**(48), 9274–9282.

15 L. Fu, K. Zhang, W. Zhang, J. Chen, Y. Deng, Y. Du and N. Tang, Synthesis and intrinsic magnetism of bilayer graphene nanoribbons, *Carbon*, 2019, **143**, 1–7.

16 Y. Li, Z. Zhou, S. Zhang and Z. Chen, MoS_2 nanoribbons: high stability and unusual electronic and magnetic properties, *J. Am. Chem. Soc.*, 2008, **130**(49), 16739–16744.

17 V. Barone and J. E. Peralta, Magnetic boron nitride nanoribbons with tunable electronic properties, *Nano Lett.*, 2008, **8**(8), 2210–2214.

18 S. Prucnal, A. Hashemi, M. Ghorbani-Asl, R. Hübner, J. Duan, Y. Wei, D. Sharma, D. R. Zahn, R. Ziegenrücker, U. Kentsch, *et al.*, Chlorine doping of $MoSe_2$ flakes by ion implantation, *Nanoscale*, 2021, **13**(11), 5834–5846.

19 M. N. Bui, S. Rost, M. Auge, J.-S. Tu, L. Zhou, I. Aguilera, S. Blügel, M. Ghorbani-Asl, A. V. Krasheninnikov, A. Hashemi, *et al.*, Low-energy se ion implantation in MoS_2 monolayers, *npj 2D Mater. Appl.*, 2022, **6**(1), 42.

20 J. Zhou, J. Lin, H. Sims, C. Jiang, C. Cong, J. A. Brehm, Z. Zhang, L. Niu, Y. Chen, Y. Zhou, *et al.*, Synthesis of Co-doped MoS_2 monolayers with enhanced valley splitting, *Adv. Mater.*, 2020, **32**(11), 1906536.

21 T. Wu, H. Shen, L. Sun, B. Cheng, B. Liu and J. Shen, Nitrogen and boron doped monolayer graphene by chemical vapor deposition using polystyrene, urea and boric acid, *New J. Chem.*, 2012, **36**(6), 1385–1391.

22 D. M. Hoat, R. Ponce-Perez, C. V. Ha and J. Guerrero-Sanchez, Controlling the electronic and magnetic properties of the GeAs monolayer by generating Ge vacancies and doping with transition-metal atoms, *Nanoscale Adv.*, 2024, **6**, 3602–3611.

23 J. Ren, H. Zhang and X. Cheng, Electronic and magnetic properties of all 3d transition-metal-doped ZnO monolayers, *Int. J. Quantum Chem.*, 2013, **113**(19), 2243–2250.

24 P. T. Bui, V. Van On, J. Guerrero-Sanchez and D. Hoat, Functionalization of boron phosphide monolayers for
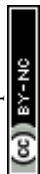
spintronic applications by doping with alkali and alkaline earth metals, *J. Phys. D: Appl. Phys.*, 2024, **57**(13), 135310.

25 B. N. N. Thi, C. V. Ha, N. T. H. Lien, J. Guerrero-Sanchez and D. Hoat, Doping-mediated electronic and magnetic properties of graphene-like ionic NaX (X= F and Cl) monolayers, *Phys. Chem. Chem. Phys.*, 2023, **25**(47), 32569–32577.

26 H. Zheng, J. Zhang, B. Yang, X. Du and Y. Yan, A first-principles study on the magnetic properties of nonmetal atom doped phosphorene monolayers, *Phys. Chem. Chem. Phys.*, 2015, **17**(25), 16341–16350.

27 A.-M. Hu, L.-l. Wang, W.-Z. Xiao, G. Xiao and Q.-Y. Rong, Electronic structures and magnetic properties in nonmetallic element substituted MoS_2 monolayer, *Comput. Mater. Sci.*, 2015, **107**, 72–78.

28 M. Chhowalla, Z. Liu and H. Zhang, Two-dimensional transition metal dichalcogenide (TMD) nanosheets, *Chem. Soc. Rev.*, 2015, **44**(9), 2584–2586.

29 N. Huo, Y. Yang and J. Li, Optoelectronics based on 2D TMDs and heterostructures, *J. Semicond.*, 2017, **38**(3), 031002.

30 H. Li, J. Wu, Z. Yin and H. Zhang, Preparation and applications of mechanically exfoliated single-layer and multilayer MoS_2 and WSe_2 nanosheets, *Acc. Chem. Res.*, 2014, **47**(4), 1067–1075.

31 L. Ottaviano, S. Palleschi, F. Perrozzi, G. D'Olimpio, F. Priante, M. Donarelli, P. Benassi, M. Nardone, M. Gonchigsuren, M. Gombosuren, *et al.*, Mechanical exfoliation and layer number identification of MoS_2 revisited, *2D Materials*, 2017, **4**(4), 045013.

32 X. Wang, Y. Gong, G. Shi, W. L. Chow, K. Keyshar, G. Ye, R. Vajtai, J. Lou, Z. Liu, E. Ringe, *et al.*, Chemical vapor deposition growth of crystalline monolayer $MoSe_2$, *ACS Nano*, 2014, **8**(5), 5125–5131.

33 F. G. Aras, A. Yilmaz, H. G. Tasdelen, A. Ozden, F. Ay, N. K. Perkgoz and A. Yeltik, A review on recent advances of chemical vapor deposition technique for monolayer transition metal dichalcogenides (MX_2: Mo, W; S, Se, Te), *Mater. Sci. Semicond. Process.*, 2022, **148**, 106829.

34 Y. Wang, L. Zhou, M. Zhong, Y. Liu, S. Xiao and J. He, Two-dimensional noble transition-metal dichalcogenides for nanophotonics and optoelectronics: Status and prospects, *Nano Res.*, 2022, **15**(4), 3675–3694.

35 X. Yu, P. Yu, D. Wu, B. Singh, Q. Zeng, H. Lin, W. Zhou, J. Lin, K. Suenaga, Z. Liu, *et al.*, Atomically thin noble metal dichalcogenide: a broadband mid-infrared semiconductor, *Nat. Commun.*, 2018, **9**(1), 1545.

36 C. Long, Y. Liang, H. Jin, B. Huang and Y. Dai, $PdSe_2$: flexible two-dimensional transition metal dichalcogenides monolayer for water splitting photocatalyst with extremely low recombination rate, *ACS Appl. Energy Mater.*, 2018, **2**(1), 513–520.

37 D. Zhao, S. Xie, Y. Wang, H. Zhu, L. Chen, Q. Sun and D. W. Zhang, Synthesis of large-scale few-layer PtS_2 films by chemical vapor deposition, *AIP Adv.*, 2019, **9**(2), 025225.

38 J. Lu, X. Zhang, G. Su, W. Yang, K. Han, X. Yu, Y. Wan, X. Wang and P. Yang, Large-area uniform few-layer PtS_2:

Synthesis, structure and physical properties, *Mater. Today Phys.*, 2021, **18**, 100376.

39 R. A. B. Villaos, C. P. Crisostomo, Z.-Q. Huang, S.-M. Huang, A. A. B. Padama, M. A. Albao, H. Lin and F.-C. Chuang, Thickness dependent electronic properties of Pt dichalcogenides, *npj 2D Mater. Appl.*, 2019, **3**(1), 2.

40 G. Liu, Y. Gan, R. Quhe and P. Lu, Strain dependent electronic and optical properties of PtS_2 monolayer, *Chem. Phys. Lett.*, 2018, **709**, 65–70.

41 Y. Ji, Y. Liu, Y. Xu, L. Liu and Y. Chen, Electronic and optical properties of sulfur vacancy-defect monolayer PtS_2: A first-principles study, *Mater. Chem. Phys.*, 2020, **255**, 123588.

42 H. Yoo, K. Heo, M. H. R. Ansari and S. Cho, Recent advances in electrical doping of 2D semiconductor materials: Methods, analyses, and applications, *Nanomaterials*, 2021, **11**(4), 832.

43 D. Li, Y. Niu, H. Zhao, C. Liang and Z. He, Electronic and magnetic properties of 3d-metal trioxides superhalogen cluster-doped monolayer MoS_2: a first-principles study, *Phys. Lett. A*, 2014, **378**(22–23), 1651–1656.

44 N. Feng, W. Mi, Y. Cheng, Z. Guo, U. Schwingenschlögl and H. Bai, First principles prediction of the magnetic properties of Fe-X_6 (X= S, C, N, O, F) doped monolayer MoS_2, *Sci. Rep.*, 2014, **4**(1), 3987.

45 M. Rafique, Y. Shuai, H.-P. Tan and M. Hassan, Structural, electronic and magnetic properties of 3d metal trioxide clusters-doped monolayer graphene: a first-principles study, *Appl. Surf. Sci.*, 2017, **399**, 20–31.

46 W. Kohn and L. J. Sham, Self-consistent equations including exchange and correlation effects, *Phys. Rev.*, 1965, **140**(4A), A1133.

47 G. Kresse and J. Furthmüller, Efficiency of ab-initio total energy calculations for metals and semiconductors using a plane-wave basis set, *Comput. Mater. Sci.*, 1996, **6**(1), 15–50.

48 G. Kresse and J. Furthmüller, Efficient iterative schemes for ab initio total-energy calculations using a plane-wave basis set, *Phys. Rev. B: Condens. Matter Mater. Phys.*, 1996, **54**(16), 11169.

49 J. P. Perdew, K. Burke and M. Ernzerhof, Generalized gradient approximation made simple, *Phys. Rev. Lett.*, 1996, **77**(18), 3865.

50 S. L. Dudarev, G. A. Botton, S. Y. Savrasov, C. Humphreys and A. P. Sutton, Electron-energy-loss spectra and the structural stability of nickel oxide: An LSDA+U study, *Phys. Rev. B*, 1998, **57**(3), 1505.

51 Y. Wang, S. Li and J. Yi, Transition metal-doped tin monoxide monolayer: a first-principles study, *J. Phys. Chem. C*, 2018, **122**(8), 4651–4661.

52 T. V. Vu, V. H. Chu, J. Guerrero-Sanchez and D. M. Hoat, Regulating the electronic and magnetic properties of a SnSSe janus monolayer toward optoelectronic and spintronic applications, *ACS Appl. Electron. Mater.*, 2024, **6**(5), 3647–3656.

53 H. J. Monkhorst and J. D. Pack, Special points for Brillouin-zone integrations, *Phys. Rev. B: Solid State*, 1976, **13**(12), 5188.

54 G. Henkelman, A. Arnaldsson and H. Jónsson, A fast and robust algorithm for Bader decomposition of charge density, *Comput. Mater. Sci.*, 2006, **36**(3), 354–360.

55 E. Sanville, S. D. Kenny, R. Smith and G. Henkelman, Improved grid-based algorithm for Bader charge allocation, *J. Comput. Chem.*, 2007, **28**(5), 899–908.

56 M. Kashif, N. Anjum, A. Shahzad, A. Rasheed, M. Imran and A. Manzoor, Tuning the electronic and optical properties of the ZrS_2/PtS_2 van der Waals heterostructure by an external electric field and vertical strain, *ACS omega*, 2022, **7**(37), 33453–33460.

57 A. Togo, L. Chaput, T. Tadano and I. Tanaka, Implementation strategies in phonopy and phono3py, *J. Phys.: Condens. Matter*, 2023, **35**(35), 353001.

58 S. Nosé, A unified formulation of the constant temperature molecular dynamics methods, *J. Chem. Phys.*, 1984, **81**(1), 511–519.

59 W. G. Hoover, Canonical dynamics: Equilibrium phase-space distributions, *Phys. Rev. A: At., Mol., Opt. Phys.*, 1985, **31**(3), 1695.

60 F. Mouhat and F.-X. Coudert, Necessary and sufficient elastic stability conditions in various crystal systems, *Phys. Rev. B: Condens. Matter Mater. Phys.*, 2014, **90**(22), 224104.

61 A. V. Krukau, O. A. Vydrov, A. F. Izmaylov and G. E. Scuseria, Influence of the exchange screening parameter on the performance of screened hybrid functionals, *J. Chem. Phys.*, 2006, **125**(22), 224106.

62 M. Sajjad, N. Singh and U. Schwingenschlögl, Strongly bound excitons in monolayer PtS_2 and $PtSe_2$, *Appl. Phys. Lett.*, 2018, **112**(4), 043101.

63 I. Choudhuri, P. Bhauriyal and B. Pathak, Recent advances in graphene-like 2D materials for spintronics applications, *Chem. Mater.*, 2019, **31**(20), 8260–8285.

64 X. Li and J. Yang, First-principles design of spintronics materials, *Natl. Sci. Rev.*, 2016, **3**(3), 365–381.